Distributed UAV Swarm Formation and Collision Avoidance Strategies Over Fixed and Switching Topologies

Jia Wu, Chunbo Luo*, *Member, IEEE,* Yang Luo, and Ke Li, *Member, IEEE*

***Abstract*—This paper proposes a controlling framework for multiple unmanned aerial vehicles (UAVs) to integrate the modes of formation flight and swarm deployment over fixed and switching topologies. Formation strategies enable UAVs to enjoy key collective benefits including reduced energy consumption, but the shape of the formation and each UAV's freedom are significantly restrained. Swarm strategies are thus proposed to maximise each UAV's freedom following simple yet powerful rules. This paper investigates the integration and switch between these two strategies, considering the deployment environment factors such as poor network conditions and unknown and often highly mobile obstacles. We design a distributed formation controller to guide multiple UAVs in orderless states to swiftly reach an intended formation. Inspired by starling birds and similar biological creatures, a distributed collision avoidance controller is proposed to avoid unknown and mobile obstacles. We further illustrated the stability of the controllers over both fixed and switching topologies. Experiment results confirm the effectiveness of the framework.**

***Index Terms*—UAV, formation, swarm intelligence, collision avoidance**

I. Introduction

UNMANNED aerial vehicles (UAVs) have become increasingly important in many real-world applications, such as precise agriculture, disaster relief, emergency communications and cargo transportation [1]–[4]. Comparing with a single UAV, a herd of multiple UAVs can accomplish tasks more efficiently and achieve improved overall robustness with effective control and communication strategies. Similar phenomena have been observed in biological world where birds and fish often create formations spontaneously to gain aerodynamic advantages or avoid dangerous predators [5] (See Fig. 1). Out of these versatile species, starling birds are especially famous for forming versatile shapes, leading to significant biological studies and even becoming famous attractions to visitors, e.g. the starling birds in Rome [6]. Inspired by these biological behaviours, this paper studies the control strategies for formation flight and collision avoidance of a group of UAVs.

Formation and swarm strategies usually assume and treat individual UAV differently, and thus seamless integration between the two modes at each UAV poses challenges for controller design. Under formation strategies, UAVs' paths are often devised in advance where each UAV is coordinated with its neighbours to achieve a desired formation along the planned paths [7]–[9]. The consensus mechanism among UAVs which are often modelled as multi-agent systems is a common algorithm to achieve formations [7], [8], [10]. Highly effective control strategies have been proposed for UAVs to coordinate their states, including position and velocity, to achieve the consensus state where the intended geometric shape and a strictly ordered formation could be achieved [7], [8], [10]. Under these strategies, individual UAV's velocity and other mobile parameters harmonises with its neighbours and their relative positions become stable. Efficient formation controlling models have also been proposed. The leader-follower formation models are widely applied for controlling UAV formations, under which the follower UAVs track the state of a leader UAV to reach the consensus orchestrated by the strategy [11], [12]. In contrast, virtual structure approaches have no explicit leader and instead steer UAVs to follow a virtual point of the rigid body [13], [14]. Furthermore, artificial potential field methods introduce a virtual field that confines the UAV herd so that they can keep stable formation [15], [16]. These formation strategies show excellent controlling capability, but are lack of individual flexibility. This often happens in practical UAV deployment scenarios where individual intelligence is in need. For example, the rigid shapes formed by formation approaches lack the flexibility to avoid scattered obstacles, particularly the mobile and hostile ones.

Swarm strategies usually treat UAVs as self-organized agents with individual intelligence. Collective intelligence thus emerges spontaneously by simply interacting, in a similar way like large animal groups such as bees or ants [17]. Under these strategies, each individual determines its next action by interacting with some nearest neighbours. Rich swarm

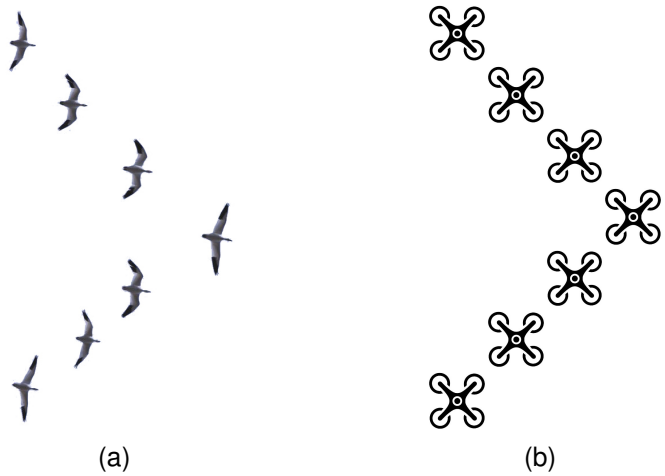

Fig. 1. Synchronized flight of bird flocks and formation flight of a group of UAVs.

algorithms have been proposed to simulate swarm behaviours. Typical examples include particle swarm optimization from studying the predation behaviour of birds [18] [19] and ant colony algorithms to imitate the behaviours of ant populations [20]. Swarm behaviours of animals have been extensively studied in existing literatures, e.g. [21]. The characteristics of animal swarms' movement in nature are summarised into three key rules: collision avoidance, velocity matching, and flock centering. There have been some successful applications of swarm strategies for UAVs reported in the literature. For example, authors of [22] introduced a group of UAVs following an evolutionary framework which achieves optimised deployment at the presence of static barriers and perturbations. A bio-inspired robust and self-repairing formation controller was proposed in [23], which defines a virtual container set to control the formation shape. Each agent is treated as a gas molecule that diffuses in the container and the group in the virtual container does not follow a coordinated speed and direction of motion. Agents with relatively simple behaviours could enjoy individual intelligence and achieve coarsely ordered state without centralised control. Bio-inspired swarm approaches assuming individuals with high freedom are thus difficult to achieve strict orderly formation [23], [24], and will inevitably lead to decreased efficiency in the deployment and energy consumption, which are key to the stringent UAV platforms, particularly multirotors.

In practice, UAV swarms may be attacked by or collided with flying birds when performing tasks, so complex deployment scenarios often require a group of UAVs to be capable of maintaining an orderly formation during flight and also exploiting individual intelligence to avoid mobile obstacles such as birds or intruders. Therefore, this paper proposes an integrated deployment framework based on the observation that individuals in a distributed system are only responsible for themselves, and under the proper rules, they can also fly in formation and avoid obstacles autonomously like birds. The theoretical framework includes the evolved formation flight for energy saving and the evasion mechanism inspired by the flocks of starlings that form elegant shapes to avoid predators [25]. We thus propose two controllers, i.e., a formation controller and a collision avoidance controller. Compared with existing research [7], [8], [23]–[27] that treated formation and swarm intelligence of UAVs individually, our proposed distributed control framework integrates the formation mode and swarm mode to effectively solve UAVs' flight formation and obstacle avoidance problems. In addition, the formation controller in this paper also gives the convergence rate function over switching topologies of UAVs system, which reflects the speed of achieving formation and has not been considered in [7], [8]. To avoid collision among agents and obstacle during the flight, artificial potential field method is used in [26], [27], which assume obstacles are static in the environment. Our collision avoidance controller can steer UAVs to avoid unknown and dynamic obstacles, inspired by the natural behaviour of starling birds. The main contributions of this paper are summarised below:

1) We firstly proposed a distributed control framework for multiple UAVs to integrate the formation mode and swarm mode over fixed and switching topologies, forming an intelligent system in which formation and obstacle avoidance functions can be freely converted depending on whether there are obstacles. The switching between the two modes shows agile and robust performance, benefited from the distributed system structure.
2) We prove the convergence of the formation controller over fixed and switching topologies and obtain the specific convergence rate function of the system that reflects the speed of achieving formation.
3) Inspired by natural behaviour of starling birds, the collision avoidance controller is proposed, which can protect UAVs from the obstacle and avoid collisions inside the UAV swarm, even when UAVs encounter a mobile obstacle.

The remainder of this paper is organized as follows. The network model of the UAV swarm is given in Section II. Section III introduces the two types of controllers, i.e. formation controller and collision avoidance controller. In Section IV, simulation examples are provided to illustrate the models and verify the correctness of the theoretical results. Section V concludes this paper.

II. Preliminaries

The network topology graph $\mathcal{G} = \{\mathcal{V}, \mathcal{E}, W\}$ is used to describe the wireless links among UAVs, where $\mathcal{V} = \{1, 2, ..., N\}$ is the set of N nodes and $\mathcal{E} = \{(i, j)|i, j \in \mathcal{V}\}$ is the set of links. $W = \left[w_{ij}\right] \in R^{N\times N}$ is the adjacent matrix of the graph with $w_{ij} = 1$ if the link (j, i) exists, otherwise $w_{ij} = 0$. Each node represents a UAV and each edge (j, i) denotes the communication link from the jth UAV to the ith UAV. We do not consider the self-loop, i.e., $w_{ii} = 0, i = 1, ..., N$. This paper assumes the graph is unidirectional, meaning the two UAVs of a link can communicate with each other and the link is bidirectional. For an undirected graph, let $d_i = \sum_{j=1}^{N} w_{ij}$, and we have the degree matrix $D = \text{diag}\{d_1, d_2, \ldots, d_N\}$. The Laplacian matrix is defined as $L = D - W$.

TABLE I
LIST OF KEY SYMBOLS.

Symbol	Meaning
$\mathbb{Z}$	Natural number set
$\mathbb{N}$	Positive integer set
I_n	Identity matrix with a dimension n
R^n	n-dimension vector
$\|X\|$	Euclidean norm or spectral norm of X
X^{T}	Conjugate transpose of X
$\lambda_i(A)$	i-th eigenvalue of square matrix A
$\rho(A)$	Spectral radius of square matrix A (= $\max_i \|\lambda_i\|$)
$\otimes$	Kronecker product
$\lfloor x \rfloor$	Largest integer not greater than x

A path from the node i to the node j consists of a series of links $(i,i_1),(i_1,i_2),\ldots,(i_n,j)$. The graph $\mathcal{G}$ is called a connected graph if at least one path exists between any two nodes. For a disconnected graph, a maximal connected subgraph of a undirected graph is called a connected component. If the graph $\mathcal{G}$ is connected, its eigenvalues satisfy $0 = \lambda_1 \leq \lambda_2 \leq \ldots \leq \lambda_N$. The set of adjacent nodes of node i is denoted by $\mathcal{N}_i = \{j \in V | w_{ij} = 1\}$. Because the links established by UAVs are often bidirectional, we mainly consider the undirected graph in this paper.

The key symbols are listed in Table I.

Considering position and velocity of UAVs in the swarm, we use a second-order integrator to model the UAV system, where we treat each UAV as a particle, like in [12], [27], and the main dynamic characteristics of the UAV will not affect the performance of the following formation controller and the obstacle avoidance controller. The dynamic equation of each UAV is as follows

$$\begin{cases} x_i(t+1) = x_i(t) + \sigma v_i(t) \\ v_i(t+1) = v_i(t) + \sigma u_i(t) \end{cases} \tag{1}$$

where $x_i(t) \in R^n$ and $v_i(t) \in R^n$ represent the position and velocity of UAV i, respectively. $u_i(t) \in R^n$ is the control input of velocity, and $\sigma > 0$ is the control gain.

Remark 1. *σ increases control flexibility of the UAV swarm. If σ approaches zero, the second-order discrete time system (1) is approximately equivalent to a second-order continuous system as follows*

$$\begin{cases} \dot{x}_i(t) = v_i(t) \\ \dot{v}_i(t) = u_i(t) \end{cases}$$

and σ can be regard as sampling time in this case. On the other hand, if σ is equal to 1, the system becomes a normal discrete time system as follows

$$\begin{cases} x_i(t+1) = x_i(t) + v_i(t) \\ v_i(t+1) = v_i(t) + u_i(t) \end{cases}$$

Let $\xi_i(t) = [x_{i1}(t), v_{i1}(t), \cdots, x_{in}(t), v_{in}(t)]^{\mathrm{T}} \in R^{2n}$. Then, the second-order system is converted into the following first-order system:

$$\xi_i(t+1) = \xi_i(t) + \sigma\left(A\xi_i(t) + Bu_i(t)\right) \tag{2}$$

where $A = I_n \otimes \begin{bmatrix} 0 & 1 \\ 0 & 0 \end{bmatrix}$ and $B = I_n \otimes \begin{bmatrix} 0 \\ 1 \end{bmatrix}$.

The shape of the intended formation of the ith UAV is denoted by $f_i = \left[f_{ix_1}(t), 0, \cdots, f_{ix_n}(t), 0\right]^{\mathrm{T}} \in R^{2n}$, where $f_{ix_j}(t), j = 1, \cdots, n$ represents the intended formation position of the ith UAV. The trajectory of UAVs during formation is represented by $h(t) = \left[h_{x_1}(t), h_{v_1}(t), \cdots, h_{x_n}(t), h_{v_n}(t)\right]^{\mathrm{T}} \in R^{2n}$, where h_{x_j} and $h_{v_j}, j = 1, \cdots n$ represent the central position and the overall velocity of the formation in the jth dimension, respectively.

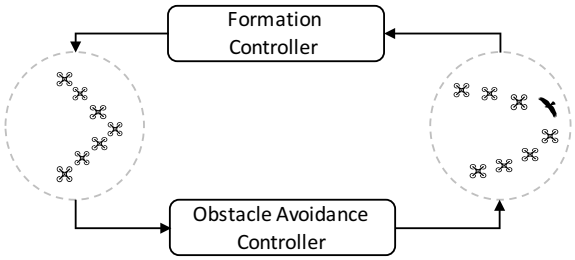

Fig. 2. The conceptual framework.

Definition 1. *If $\lim_{t\to\infty}(\xi_i(t) - f_i - h(t)) = 0$ is satisfied, the intended formation is achieved.*

III. THE PROPOSED FRAMEWORK

This section delineates the proposed framework for deploying multiple UAVs step by step. We firstly introduce the formation controller over a fixed topology. Considering the case that some communication links may be broken influenced by poor communication environment, we further study the controller over switching topologies. The distributed collision avoidance controller is then proposed with the inspiration from swarm behaviours of starling birds over both fixed and switching topologies. The conceptual framework is shown in Fig. 2.

A. Formation controller

1) Fixed network topology: Firstly, we start from the case of a fixed network topology. Considering a distributed system, the formation controller of each UAV uses the relative position and relative velocity information with its neighbors to realize the desired formation. A distributed formation control protocol is proposed as follows

$$u_i(t) = K\sum_{j=1}^{N} w_{ij}\left(\left(\xi_j(t) - \xi_i(t)\right) - \left(f_j - f_i\right)\right) \tag{3}$$

where $K \in R^{n\times 2n}$ is the feedback control matrix. In practice, UAVs will communicate with their neighbors to obtain the relative states (position and velocity) for the formation. The communication systems for multiple UAVs have been extensively studied, such as [28]–[32]. A practical way is to establish multicast or broadcast air to air wireless links within the formation [28] and maintain a communication network where UAVs share the state information. This method has been successfully used in practical UAV systems [30], [31]. Based on the shared information, UAVs can obtain the relative states information of the formation UAVs [30]–[32].

The following Lemma III.1 helps prove the stability of the system.

Lemma III.1. *([33]) For any square matrix $M \in R^{n\times n}$ and with $\epsilon > 0$, there is*

$$\|M^t\| \le s\nu^t, t \in \mathbb{N} \tag{4}$$

where $s = \sqrt{n}\left(1+\frac{2}{\epsilon}\right)^{n-1}$ is a constant closely related to the dimension of matrix M, and $\nu = \rho(M) + \epsilon\|M\|$ whose value depends on the spectral radius $\rho(M)$. If $\nu < 1$, then M is a convergent matrix.

Theorem III.1. *For a UAV system under the designed formation controller, if the fixed topology graph is connected and the elements in matrix K satisfy $\sigma k_1 < k_2 < \frac{4k_1}{\lambda_N}$ with $0 < k_1, k_2 < 1$, the intended formation can be achieved over the fixed topology.*

Proof. In order to get the expression about the whole system, we denote $\xi(t) = \left(\xi_1^{\mathrm{T}}(t), \ldots, \xi_N^{\mathrm{T}}(t)\right)^{\mathrm{T}}$ and $F = \left(f_1^{\mathrm{T}}, \ldots, f_N^{\mathrm{T}}\right)^{\mathrm{T}}$. Combined with the controller (3), the UAV system (2) has the following matrix expression

$$\xi(t+1) = \xi(t) + (I_N \otimes \sigma A)\,\xi(t) - (L \otimes \sigma BK)(\xi(t) - F)$$

Denote $\hat{\delta}_i(t) = \xi_i(t) - f_i$ and $\hat{\delta}(t) = \left(\hat{\delta}_1^{\mathrm{T}}(t), \hat{\delta}_2^{\mathrm{T}}(t), \ldots, \hat{\delta}_N^{\mathrm{T}}(t)\right)^{\mathrm{T}}$. Then, we have

$$\begin{aligned}\hat{\delta}(t+1) = \hat{\delta}(t) + (I_N \otimes \sigma A)\,\hat{\delta}(t) - (L \otimes \sigma BK)\hat{\delta}(t) \\ + (I_N \otimes \sigma A)\,F\end{aligned} \tag{5}$$

According to the property of the Laplacian matrix L, there exists unitary matrix V^{-1} such that $J = V^{-1}LV = \mathrm{diag}\{0, \tilde{J}\}$ with $\tilde{J} = \mathrm{diag}\{\lambda_2, \lambda_3, \ldots, \lambda_N\}$. Denote $V = [v_1, v_2, \ldots, v_N]$ with v_i being the unitized normalized eigenvector corresponding to the eigenvalue λ_i. In addition, we know $v_1 = \frac{1_N}{\sqrt{N}}$ because $\lambda_1 = 0$. We define $V^{-1} = \begin{bmatrix} \tilde{v}_1; \tilde{v}_2; & \ldots; \tilde{v}_N \end{bmatrix} = \begin{bmatrix} \tilde{v}_1; & \tilde{V} \end{bmatrix}$, where $\tilde{v}_i, i = 2, \ldots N$ is the row eigenvector and $\tilde{V} = \begin{bmatrix} \tilde{v}_2; & \ldots; \tilde{v}_N \end{bmatrix}$. Denote $\zeta(t) = \left(V^{-1} \otimes I_n\right)\hat{\delta}(t) = \left[(\tilde{v}_1 \otimes I_n)\,\hat{\delta}(t); \quad \left(\tilde{V} \otimes I_n\right)\hat{\delta}(t)\right]$ and it can be written as

$$\begin{aligned}\zeta(t+1) = \zeta(t) + (I_N \otimes \sigma A)\,\zeta(t) - \left(V^{-1}LV \otimes \sigma BK\right)\zeta(t) \\ + \left(V^{-1} \otimes \sigma A\right)F\end{aligned} \tag{6}$$

Let $\omega(t) = (\tilde{v}_1 \otimes I_n)\,\hat{\delta}(t)$ and $\psi(t) = \left(\tilde{V} \otimes I_n\right)\hat{\delta}(t)$, and we can derive

$$\omega(t+1) = \omega(t) + \sigma A\omega(t) + (\tilde{v}_1 \otimes \sigma A)\,F \tag{7}$$

$$\begin{aligned}\psi(t+1) = \psi(t) + (I_{N-1} \otimes \sigma A)\,\psi(t) - (\tilde{J} \otimes \sigma BK)\psi(t) \\ + (\tilde{V} \otimes \sigma A)F\end{aligned} \tag{8}$$

Then, we define $\tilde{\omega}(t) = (V \otimes I_n)\,[\omega(t) \quad 0]^{\mathrm{T}}$ and $\hat{\omega}(t) = (V \otimes I_n)\begin{bmatrix} 0 & \psi(t) \end{bmatrix}^{\mathrm{T}}$. Further, we have

$$\begin{aligned}\tilde{\omega}(t) + \hat{\omega}(t) &= (V \otimes I_n)\,[\omega(t) \quad \psi(t)]^{\mathrm{T}} \\ &= (V \otimes I_n)\,\zeta(t) \\ &= \hat{\delta}(t)\end{aligned}$$

It should be pointed out that $\tilde{\omega}(t) = \frac{1_N}{\sqrt{N}} \otimes \omega(t)$. Thus, if $\lim_{t\to\infty}\|\hat{\omega}(t)\| = 0$ is satisfied, we have $\lim_{t\to\infty}\|\delta(t) - \tilde{\omega}(t)\| = \lim_{t\to\infty}\left\|\xi(t) - F - \frac{1_N}{\sqrt{N}} \otimes \omega(t)\right\| = 0$. That is, the desired formation is achieved with the center trajectory $h(t) = \frac{1_N}{\sqrt{N}} \otimes \omega(t)$ that also reflects the formation trajectory. Since V is a unitary matrix, $\lim_{t\to\infty}\|\hat{\omega}(t)\| = 0$ is equivalent to $\lim_{t\to\infty}\|\psi(t)\| = 0$. Based on the definition of F, we have $\left(\tilde{V} \otimes \sigma A\right)F = 0$. Therefore, we only need to analyze the convergence of the equation (8), and it can be written as

$$\psi(t+1) = \left(I_{N-1} \otimes \tilde{A} - \sigma\tilde{J} \otimes BK\right)\psi(t) \tag{9}$$

where $\tilde{A} = I_n \otimes I_2 + \sigma A$. Then, the distributed formation control problem is transformed into a system convergence analysis problem.

Let $\psi(t) = \left[\psi_1^T(t), \ldots, \psi_N^T(t)\right]$. From equation (8), we have $\psi_i(t+1) = (\tilde{A} - \sigma\lambda_i BK)\psi_i(t), i \ge 2$. Then, the design of feedback control is crucial to ensure a stable system. The system need to satisfy $\rho(\tilde{A} - \sigma\lambda_i BK) < 1$ with the designed K. By analyzing the characteristics of the system matrices A and B, we propose a strategy for designing the feedback matrix K.

In order to simplify the formula, we consider one dimension of ith UAV for the following analysis, but the theoretical results are applicable to any dimension of x_i. Then, we have $\tilde{A} = \begin{bmatrix} 1 & \sigma \\ 0 & 1 \end{bmatrix}$ and $B = \begin{bmatrix} 0 \\ 1 \end{bmatrix}$. Denote $K = \begin{bmatrix} k_1 & k_2 \end{bmatrix}$. Hence, we can calculate

$$\left|\lambda(\tilde{A} - \sigma\lambda_i BK)\right| = \left|1 - \frac{\sigma\lambda_i k_2}{2} \pm \sqrt{\frac{\sigma^2\lambda_i^2 k_2^2}{4} - \sigma^2\lambda_i k_1}\right| < 1 \tag{10}$$

Because the topology is connected in this case, we have $\lambda_i \ne 0, i \ge 2$. In order to ensure that the inequality (10) has a solution, we have $\frac{\sigma^2\lambda_i^2 k_2^2}{4} - \sigma^2\lambda_i k_1 < 0$. Further, to solve $\left|\lambda(\tilde{A} - \sigma\lambda_i BK)\right|^2 < 1$, we get $1 + \sigma^2\lambda_i k_1 - \sigma\lambda_i k_2 < 1$. Then, we can obtain that the sufficient condition for a stable system is $\sigma k_1 < k_2 < \frac{4k_1}{\lambda_N}$ with $0 < k_1, k_2 < 1$ by solving the inequality. According to Lemma III.1, we get

$$\begin{aligned}\|\psi_i(t+1)\| &\le \left\|\left(\tilde{A} - \sigma\lambda_i \otimes BK\right)^{t+1}\right\|\|\psi_i(0)\| \\ &\le s\nu^{t+1}\|\psi_i(0)\|\end{aligned} \tag{11}$$

with $\max_{\lambda_i \ne 0}\rho\left(\tilde{A} - \sigma\lambda_i BK\right) \le \nu < 1$. Thus, we can see $\lim_{t\to\infty}\|\psi_i(t)\| = 0$. That is, $\lim_{t\to\infty}\|\psi(t)\| = 0$, and the intended formation can be achieved under the designed formation controller.

Next we analyze the convergence performance of the system. According to (11), we define the convergence rate function as $o(t) = s\nu^t$. The smaller the convergence rate function value, the faster the system converges.

The proof is completed. □

Theorem III.1 provides the theoretical ground to guarantee the convergence of the designed formation controller (3) for each UAV under fixed topology.

2) Switching network topologies: In practice, the links among UAVs may fail due to poor network conditions. This will inevitably lead to topology changes. This subsection proposes the formation controller under the time-varying topology.

For the switching topologies, we consider that there are infinite time intervals $[t_k, t_{k+1}), k \in \mathbb{Z}$ with $t_0 = 0$ for $t \to \infty$.

Suppose that each time interval satisfies $t_{k+1} - t_k \geq T$ with $T > 0$. Further, there are $m+1$ nonoverlapping subintervals $\left[t_{k_j}, t_{k_{j+1}}\right), j = 0, 1, \ldots, m$ with $t_{k_0} = t_k$ and $t_{k_{m+1}} = t_{k+1}$ in each time interval $[t_k, t_{k+1})$. Note that during each subinterval $\left[t_{k_j}, t_{k_{j+1}}\right)$, the network topology graph $\mathcal{G}_j$ (i.e. switching subgraphs) is temporarily fixed until the next subinterval, and the corresponding Laplacian matrix is denoted by $L_j, j = 0, 1, \ldots, m$. Denote $\lambda_m \geq \rho(L_j), j = 0, 1, \ldots, m$. In each time interval $[t_k, t_{k+1})$, we define $\mathcal{G}_{\hat{k}} = \sum_{j=0}^{m} \mathcal{G}_j$ as the union graph, whose node set and link set are the union of the node set and link set of $\mathcal{G}_0, \mathcal{G}_1, \ldots, \mathcal{G}_m$, respectively. The jointly connected condition means that $\mathcal{G}_{\hat{k}}$ is connected.

For the case of switching topologies, the formation controller becomes

$$u_i(t) = K \sum_{j=1}^{N} w_{ij}(t) \left(\left(\xi_j(t) - \xi_i(t) \right) - \left(f_j - f_i \right) \right) \tag{12}$$

where $w_{ij}(t)$ is time-varying because each communication link is dynamic. It is worth to highlight that the fixed topology controller is a special case of this more general controller.

Assumption 1. *For each time interval $[t_k, t_{k+1})$, $G_{\hat{k}}$ is jointly connected. We assume that each broken link will try to re-establish itself and the duration of each link failure satisfies $\kappa \leq \frac{T}{2}$. This assumption is held given wireless communication channels sometimes suffer from a short period of deep fading.*

Lemma III.2. *([34]) For a simple connected graph, the maximum eigenvalue of Laplacian matrix satisfies*

$$\overline{\lambda}_N \leq \max \left\{ d_i(t) + \sqrt{d_i(t) m_i(t)} \right\}$$

where $d_i(t)$ represents the degree of node i at time t and $m_i(t) = \frac{\sum_{j \in N_i} d_j(t)}{d_i(t)}$ is called average 2-degree of node i.

Theorem III.2. *For a UAV system under the formation controller, if $\sigma k_1 < k_2 < \frac{4k_1}{\lambda_m}$ with $0 < k_1, k_2 < 1$ and Assumption 1 are satisfied, the intended formation can be achieved over switching network topologies.*

Proof. For $t \in \left[t_{k_j}, t_{k_{j+1}}\right), j = 0, 1, \ldots, m$, we have

$$\begin{aligned} \hat{\delta}(t+1) = & \left(I_N \otimes \sigma \tilde{A} - L_j \otimes \sigma BK \right) \hat{\delta}(t) \\ & + \left(I_N \otimes \sigma A \right) F \end{aligned}$$

There exists an unitary matrix V such that $V^{-1} L_j V = \text{diag}\left\{0, J_j\right\}$ with $J_j = \text{diag}\left\{\lambda_2', \lambda_3', \ldots, \lambda_N'\right\}$, and the unitized normalized eigenvector corresponding to the first eigenvalue 0 is $v_1 = \frac{1_N}{\sqrt{N}}$. Different from $\tilde{J}$, the eigenvalues $\lambda_i', i = 2, \ldots, N$ may be equal to 0 instead of always greater than 0. According to the definition of $\zeta(t)$, we get

$$\zeta(t+1) = \left(I_N \otimes \sigma \tilde{A} - J_j \otimes \sigma BK \right) \zeta(t) \tag{13}$$

Similarly, we have $\zeta(t) = \left[\left(\tilde{v}_1 \otimes I_n \right) \hat{\delta}(t) \quad \left(\tilde{V} \otimes I_n \right) \hat{\delta}(t) \right]^{\mathrm{T}} = \left[\omega(t) \quad \psi(t) \right]^{\mathrm{T}}$. We can draw the same conclusion that if $\lim_{t \to \infty} \|\psi_i(t)\| = 0$, the intended formation can be achieved. Further, we have

$$\psi_i(t+1) = \left(\tilde{A} - \sigma \lambda_i' BK \right) \psi_i(t), i = 2, \ldots, N \tag{14}$$

The node i in the switching network topologies faces two cases: $\lambda_i' \neq 0, i = 2, \ldots, N$ with the ith agent connected to the main network (largest connected subgraph) and $\lambda_i' = 0$ with the ith agent disconnected to the main network. Note that here we regard node i as the smallest numbered node on other connected subgraphs. Similarly, we consider any dimension of ith UAV and denote $K = \begin{bmatrix} k_1 & k_2 \end{bmatrix}$. When $\lambda_i' \neq 0$, let $\sigma k_1 < k_2 < \frac{4k_1}{\lambda_m}$ with $0 < k_1, k_2 < 1$. Then we have $\rho\left(\tilde{A} - \sigma \lambda_i' BK\right) < 1$. When $\lambda_i' = 0$, we have $\psi_i(t+1) = \tilde{A} \psi_i(t)$, where $\rho\left(\tilde{A}\right) = 1$. For each $t \in [t_k, t_{k+1})$, combined with Lemma III.1, we have

$$\begin{aligned} \|\psi_i(t_{k+1})\| \leq & \left\|\tilde{A}\right\|^{\kappa_1} \left\|\tilde{A} - \sigma \lambda BK\right\|^{\kappa_2} \|\psi_i(t_k)\| \\ \leq & s_1 s_2 \|\psi_i(t_k)\| \nu_1^{\kappa_1} \nu_2^{\kappa_2} \end{aligned} \tag{15}$$

where κ_1 and κ_2 respectively represent the sum of the durations of $\lambda_i' = 0$ and $\lambda_i' \neq 0$ and satisfy $\kappa_1 + \kappa_2 = t_{k+1} - t_k$; λ is any non-zero eigenvalue of Laplace matrix; s_1 and s_2 correspond to s in Lemma III.1, and ν_1 and ν_2 correspond to ν. Then, we have

$$\nu_1^{\kappa_1} \nu_2^{\kappa_2} = \left(\rho\left(\tilde{A}\right) + \epsilon \left\|\tilde{A}\right\| \right)^{\kappa_1} \left(\rho(Y) + \epsilon \|Y\| \right)^{\kappa_2}$$

where $\nu_1 = \rho\left(\tilde{A}\right) + \epsilon \left\|\tilde{A}\right\|$, $\nu_2 = \rho(Y) + \epsilon \|Y\|$ and $Y = \tilde{A} - \sigma \lambda_i BK$. In adition, we have $\rho\left(\tilde{A}\right) = 1$ and $\rho(Y) < 1$. Let $\gamma(\kappa_1, \kappa_2) = \nu_1^{\kappa_1} \nu_2^{\kappa_2}$. To make $\|\psi_i(t_{k+1})\|$ convergent, $\gamma < 1$ must be satisfied. Because we know that the bigger κ_1, the bigger γ, let $\kappa_1 \leq \kappa_2$. Then, when $\kappa_1 = \kappa_2$, we get $\overline{\gamma} = \max \gamma = \gamma(\kappa_1, \kappa_1)$. Since $\epsilon > 0$ can be a sufficiently small constant, we have

$$\begin{aligned} & \overline{\gamma} \\ = & \left[\left(\rho\left(\tilde{A}\right) + \epsilon \left\|\tilde{A}\right\| \right) \left(\rho(Y) + \epsilon \|Y\| \right) \right]^{\kappa_1} \\ = & \left[\rho(Y) + \epsilon \left(\|Y\| + \rho(Y) \left\|\tilde{A}\right\| + \epsilon \left\|\tilde{A}\right\| \|Y\| \right) \right]^{\kappa_1} \\ < & 1 \end{aligned} \tag{16}$$

Combining (15) and (16), we can define the convergence rate function as $o(t) = s_1 s_2 \overline{\gamma}^n$ in this case, where $n = \lfloor \frac{t}{t_{k+1} - t_k} \rfloor$. There is a permutation matrix P such that $P^{\mathrm{T}} L_j P = diag\left\{L_{j1}, L_{j2}, \ldots, L_{jq}\right\}$, where q is the number of connected component of switching subgraph $\mathcal{G}_j$ and $L_{ji}, i = 1, \ldots, q$ is the Laplace matrix corresponding to the connected components of $\mathcal{G}_j$. From this, we can know that if Assumption 1 is satisfied, the duration of $\lambda_i' = 0, i = 2, \cdots, N$ is less than $T/2$ in each $t \in [t_k, t_{k+1})$. That is, $\kappa_1 \leq \kappa_2$ is satisfied. Then, we can obtain $\overline{\gamma} < 1$ and $\lim_{t \to \infty} \|\psi_i(t)\| = 0$. In addition, according to Lemma III.2, we can get the appropriate value of λ_m. Then, considering $o(t)$, we can conclude that the system will achieve exponential convergence.

The proof is completed. □

Theorem III.2 provides the theoretical ground to guarantee the convergence of the designed formation controller (12) for each UAV under switching topologies.

In practice, each UAV in the group firstly uses the formation controller (12) to reach the desired formation. During the navigation stage, if a UAV i detects that a obstacle is approaching, it will switch to the following collision avoidance controller.

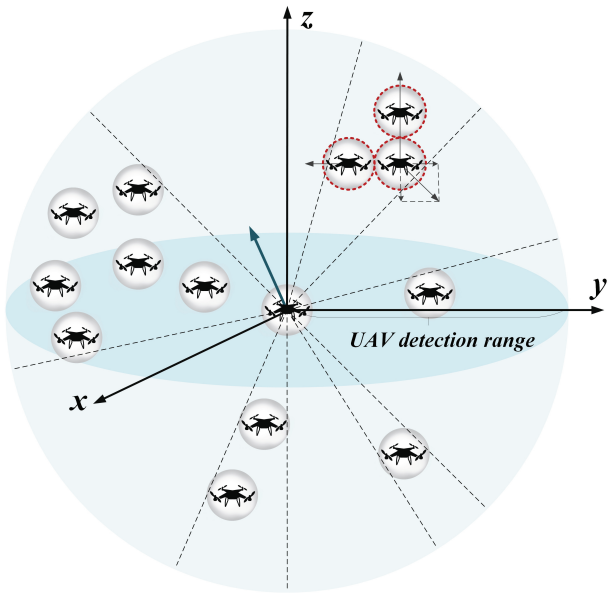

Fig. 3. A UAV swarm. The central UAV perceives its neighbors by detecting the projected shadow edges. We assume a UAV can detect the neighboring UAVs under a limited communication range indicated in the figure.

B. Distributed collision avoidance controller

During formation flight, mobile obstacles such as birds may intrude the UAV formation, endangering the UAVs whose freedom is restrained by the formation controllers. Inspired by the swarm behaviour of starling birds eluding predators, we design a distributed collision avoidance controller for the UAVs to flexibly avoid unknown and dynamic threats or obstacles during the voyage.

Fig. 3 illustrates a UAV swarm to simulate the biological behaviours of starling birds. Each UAV perceives the world in the same way as the central UAV. In the figure, the center UAV adapts its movement based on the perceived information including its distances to the obstacle and its closest neighboring UAVs. As described by Daniel J. G. Pearce and Adam M. Miller etc [25], a starling senses its neighbors by detecting the edges of the light shadows created by its neighbors. The perceived shadows are used by the starlings to adjust their flying velocities. Because each bird changes its velocity according to the behaviours of its neighbors, the whole process exhibits typical swarm characteristics.

To model such a mechanism, we design the following collision avoidance controller for each UAV, considering the distance and relative velocity to the obstacle, the relative velocity and safety distance between itself and neighboring UAVs and noises. We also consider the special case if two or more are within each other's safety distance. The model does not restrict the method used to detect obstacles or neighbor UAVs, which is a well researched topic with abundant contributions (e.g. [35], [36]).

The distributed collision avoidance controller under both fixed and switching topologies is as follows,

$$u_i(t) = \vec{a}_{i1} + \vec{a}_{i2} + \vec{a}_{i3}, \tag{17}$$

where

$$a_{i1} = \begin{cases} -a\vec{v}_i & \text{if } D < c \\ 0 & \text{if } D \geq c \end{cases}$$

$$a_{i2} = \phi_a \frac{1}{\mathcal{N}_i} \sum_{j \in \mathcal{N}_i} w_{ij}(t)\hat{v}_j(t) + \phi_p \frac{\int_{\{O_j\}} \hat{r}\, dl}{\int_{\{O_j\}} dl} + \phi_n e_i(t)$$

$$a_{i3} = \begin{cases} \vec{r}_i & \text{if } d < c_0 \\ 0 & \text{if } d \geq c_0 \end{cases}$$

- a_{i1} describes the acceleration away from the intruding obstacle. If the distance D between the ith UAV and the obstacle is less than a predefined external safe distance c, the velocity of this UAV will be adjusted by an acceleration a away from the direction of the obstacle or threat, where $\vec{v}_i$ is the unit velocity vector of the dynamic obstacle. It is used to indicate the direction of the obstacle detected by the ith UAV at this moment.
- a_{i2} guarantees the aggregation and collision avoidance among the UAV swarm. The key idea is to sheer the UAV to a direction with a lower density of UAVs. The first term on the right hand side (RHS) indicates that the velocity of the ith UAV will try to match the velocity of its neighbors, where $\hat{v}_j$ is a normalized velocity vector of the jth UAV. The second term on the RHS called the projected input shows that the moving direction of each UAV will be affected by the distribution of the surrounding UAVs as shown in Fig. 3, where $\hat{r}$ is the outward pointing unit vector along the shadows $O_j, j \in \mathbb{N}$. The shadows O_j are on the surface of the sphere of central UAV and caused by other UAVs. The integration is carried out in a spherical boundary, where the result of it is a vector indicating the direction that is represented by a blue arrow in Fig. 3. The controller also considers a noise term $e_i(t)$, which is assumed to be uncorrelated with each UAV. ϕ_a, ϕ_p and ϕ_n are controlling parameters for the velocity, aggregation, and noise, respectively, and $\phi_a + \phi_p + \phi_n = 1$.
- a_{i3} controls the extreme cases when two or more UAVs come into each other's internal safety zone during avoiding obstacles, where the internal safe zone of each UAV is represented by the diameter c_0 of the circle outside the UAV in Fig. 3. The figure also shows a simple example that three UAVs in red dotted circles are nearly within each other's safety zone (i.e., their distance almost less than the internal safe distance c_0), and the grey arrow indicates the direction of the added repulsion acceleration $\vec{r}_i$. Although the extremely dangerous scenario is rare, we design the repulsion acceleration to further avoid collision in the swarm.

$\vec{a}_{i1}$, $\vec{a}_{i2}$ and $\vec{a}_{i3}$ are unit vectors corresponding to a_{i1}, a_{i2}, and a_{i3}, respectively. By simulating the biological behaviours of starlings, the designed collision avoidance controller can

steer UAVs to be away from the unknown and mobile obstacle autonomously, and also avoid conflicts with each other.

Remark 2. *The external safe distance c is a significant factor. If it is too large, it would lead to a frequent switching between formation and collision avoidance. On the other hand, the too small external safe distance c and internal safe distance c_0 can lead to an extremely dense swarm that would make it difficult for some UAVs to avoid obstacles and cause induced collisions among UAVs [37] [38]. Generally this value should be proportional to the swarm's velocity and the maximum distance between the UAVs in formation.*

In order to clearly show the stability of the UAV swarm under the collision avoidance algorithm, we introduce the aggregation coefficient that is related to the distance between UAVs and the center of the swarm. The aggregation coefficient is defined as $C = \frac{1}{N}\|x - 1_N \otimes \bar{x}\|$, where $x = (x_1^{\mathrm{T}}, ..., x_N^{\mathrm{T}})^{\mathrm{T}}$ and $\bar{x} = \frac{1}{N}\sum_{i=1}^{N} x_i(t)$. If C is always less than a constant, it reflects that no UAV is infinitely far away from the center of the swarm and the whole process of avoiding the obstacle ensures the stability of the system.

The ith UAV will switch to the formation controller if it does not sense any obstacles. Because each UAV will try to coordinate with the neighbors' velocity under the collision avoidance controller, an individual will not break away from the swarm even if some UAVs in the system begin to obey the formation mode. That is, the UAV swarm will still maintain good aggregation during the process of switching controllers. This feature of the proposed controller will be validated in section IV.

C. The overall framework

Then, it is necessary to consider how the two controllers switch. The switching law for nonlinear arbitrary switching systems is designed in [39] and the methods of convergence analysis of such systems is studied in [39]–[41]. We also need to design the switching law that can orchestrate the switching between the two controllers and ensure the overall stability of the system at the same time. Because the framework is distributed, each individual is only responsible for its own actions even if multiple UAVs are deployed, and it will not affect the switching operation of other UAVs. Therefore, our switching law is simple, where every UAV only decides whether it needs to switch the controller, without coordination from the swarm. That is why if a single UAV fails, it will not affect other UAVs in the system. The overall controlling framework of each UAV is outlined in Algorithm 1.

Some work also focuses on the formation and obstacle avoidance framework. For example, literature [42] proposes a graph theoretical framework that allows individuals to form formations and split formations when they encounter fixed obstacles. However, our framwork that integrates the common formation control algorithms and biological swarm intelligent algorithm is different from the existing work. Each UAV is given some freedom instead of being rigidly controlled, making it more capable of responding to emergencies. Therefore, the UAV swarms can avoid the mobile obstacle like birds, and we can also ensure the stability of the whole process.

Algorithm 1 Distributed UAV formation and collision avoidance

Require: For UAV i: $x_i(0)$, initial position; $v_i(0)$, initial velocity; σ, control gain; K, control matrices; ϕ_a, ϕ_n, ϕ_p, controlling parameters; c, external safe distance to an obstacle; c_0, internal safe distance;

Ensure: Position $x_i(t)$ and velocity $v_i(t)$

function
  Estimate the communication link a_{ij}
  if no obstacle is detected **then**
    Fly under the formation controller: $u_i(t) = K\sum_{j=1}^{N} w_{ij}(t)\left(\left(\xi_j(t) - \xi_i(t)\right) - \left(f_j - f_i\right)\right)$
    Update position and velocity: $x_i(t+1) = x_i(t) + \sigma v_i(t)$, $v_i(t+1) = v_i(t) + \sigma u_i(t)$
  else
    Switch to collision avoidance controller: $u_i(t) = \vec{a}_{i1} + \vec{a}_{i2} + \vec{a}_{i3}$
    Update position and velocity: $x_i(t+1) = x_i(t) + \sigma v_i(t)$, $v_i(t+1) = v_i(t) + \sigma u_i(t)$
  end if
  return $x_i(t)$, $v_i(t)$
end function

IV. Experiments

This section presents simulation experiments to evaluate the proposed framework. As mentioned before, an adequate formation can reduce fuel consumption of UAVs, extend the flight distance and maintain robust communication links, and thus improve the deployment efficiency. To illustrate the performance of the formation controller, we demonstrate a V-shaped formation for a swarm of UAVs. Our experiments are based on 2D space but they are also applicable to 3D space according to the algorithm. Here the number of UAVs is set to 11. Note that we can have different settings for proof-of-concept purpose. Both the shape of the UAV swarm and number of UAVs can be changed.

A. Evaluation of the formation controller for UAV swarm with fixed topology

The first experiment evaluates the performance of formation controller for UAV swarms over a fixed topology. For the sake of demonstration only, we assume the UAVs are in the same plane (e.g. the x-y plane). The formation of the ith UAV is expressed as $f_i = \left[f_{ix}, 0, f_{iy}, 0\right]^{\mathrm{T}}$, where f_{ix} and f_{iy} represent the position in the X and Y directions, respectively. Then, the specific V-shaped formation for the UAVs system is designed as $f_1 = (2\sqrt{3}, 0, 0, 0)^{\mathrm{T}}$, $f_2 = (0, 0, 2, 0)^{\mathrm{T}}$, $f_3 = (0, 0, -2, 0)^{\mathrm{T}}$, $f_4 = (-2\sqrt{3}, 0, 4, 0)^{\mathrm{T}}$, $f_5 = (-2\sqrt{3}, 0, -4, 0)^{\mathrm{T}}$, $f_6 = (-4\sqrt{3}, 0, 6, 0)^{\mathrm{T}}$, $f_7 = (-4\sqrt{3}, 0, -6, 0)^{\mathrm{T}}$, $f_8 = (-6\sqrt{3}, 0, 8, 0)^{\mathrm{T}}$, $f_9 = (-6\sqrt{3}, 0, -8, 0)^{\mathrm{T}}$, $f_{10} = (-8\sqrt{3}, 0, 10, 0)^{\mathrm{T}}$, $f_{11} = (-8\sqrt{3}, 0, -10, 0)^{\mathrm{T}}$. As shown in Fig. 4, the topology of the system is fixed where each line denotes the link between the two UAVs. The initial states (position and velocity) of a UAV are randomly generated. Let $\sigma = 0.5$. The elements in the feedback matrix are designed as $k_1 = 0.4$, $k_2 = 0.39$, according to Theorem III.1. Let $A = I_2 \otimes \begin{bmatrix} 0 & 1 \\ 0 & 0 \end{bmatrix}$, $B = I_2 \otimes \begin{bmatrix} 0 \\ 1 \end{bmatrix}$,

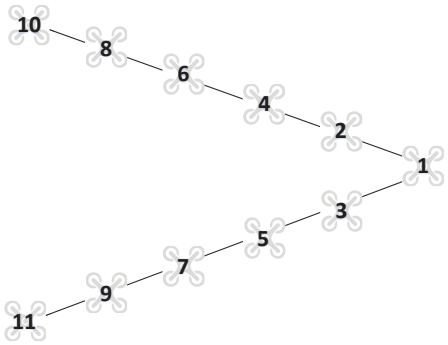

Fig. 4. A UAV swarm with fixed topology.

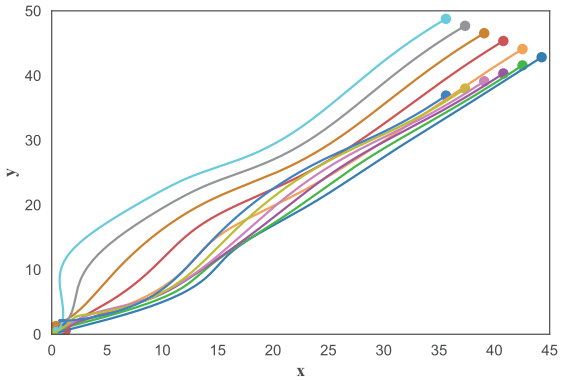

Fig. 5. Formation process of the UAV swarm over fixed topology.

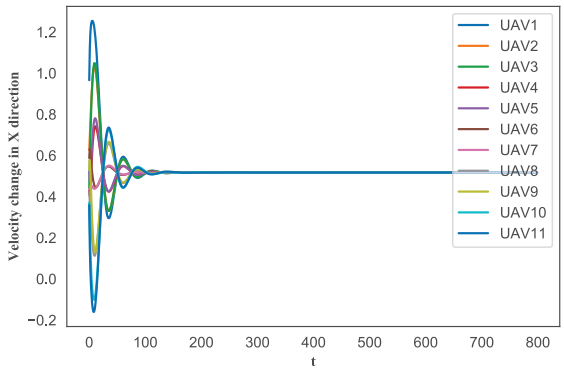

(a)

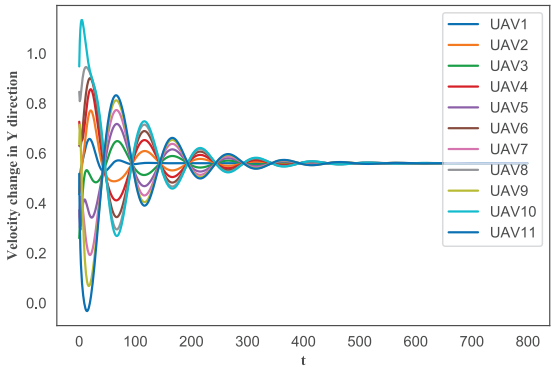

(b)

Fig. 6. The adjustment of velocities over fixed topology. (a) X dimension; (b) Y dimension.

$K = I_2 \otimes \begin{bmatrix} 0.4, & 0.39 \end{bmatrix}$, where I_2 is an identity matrix with a dimension of 2, for the X and Y dimension.

Fig. 5 shows the formation process of UAVs where each dot represents a UAV, and each line represents the corresponding trajectory. A V-shape formation is formed swiftly. Fig. 6 (a) and (b) illustrates the velocity changes of the UAVs during the formation process, in both the X and Y dimension. The two figures show that each UAV's velocity oscillates at the beginning and converges to the formation's overall velocity effectively. Fig. 5 and Fig. 6 reveal that all UAVs will finally keep V-shaped formation and move collectively with the same velocity under the formation controller.

B. Evaluation of the formation controller for UAV swarm with switching topology

This experiment evaluates the performance of the formation controller for UAV swarms over switching topologies. We assume the deployment scenario has frequent communication failures. We set the duration of each switching time interval $[t_k, t_{k+1})$ to 4 time slots. Then, each link failure may last as long as two time slots under Assumption 1. That is, we have $\kappa \leq 2$. The real-world value of each time slot can be adjusted based on the network channel conditions. For example, for a relatively stable wireless channel with line of sight connections, this value is greater than that of a channel with strong interference or frequent interruptions. Under this scenario, the connections of a swarm shown in Fig. 4 randomly fail. Fig. 7(a) and (b) give two snapshots of the network topology. Each connected component of $\mathcal{G}_j$ in these two figures is regarded as a connected subgraph. According to Lemma III.2, we can evaluate $\lambda_m = 4$. The feedback matrix K can be the same as the case of fixed topology because Theorem III.2 is satisfied.

Fig. 8 demonstrates the formation process of the UAV swarm, where topologies switched frequently during the simulation process. Compared with Fig. 5, although both of them show that the proposed controller could steer the UAVs to achieve the designed V-shape, the formation trajectory in Fig. 8 is different from that in Fig. 5. During the formation process, the change of the UAV's velocities are given in Fig. 9 (a) and (b). The scale of the change and the convergence speed are different from the fixed topology setting, because network topologies are diverse and the corresponding convergence rate function is different. Fig. 8 and Fig. 9 indicate that the UAV swarm achieves the designed formation and will fly synchronously next.

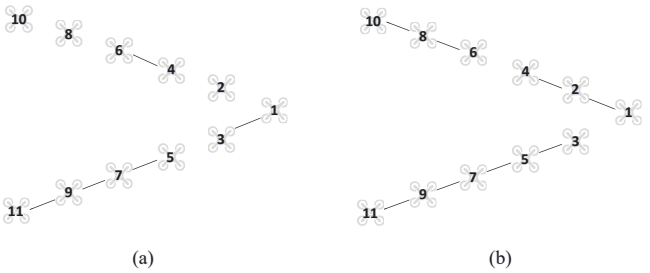

Fig. 7. Snapshots of the UAV swarm's toplogy at two randomly selected time slots.

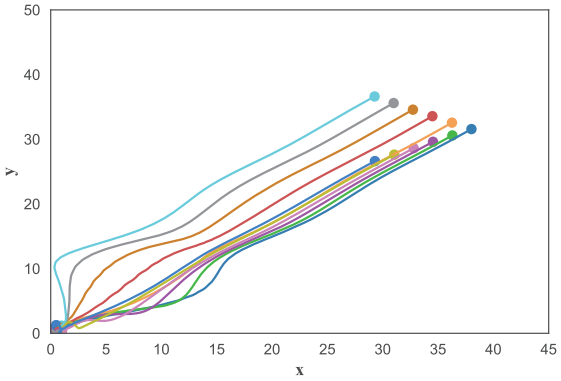

Fig. 8. Formation process of the UAV swarm over switching topologies.

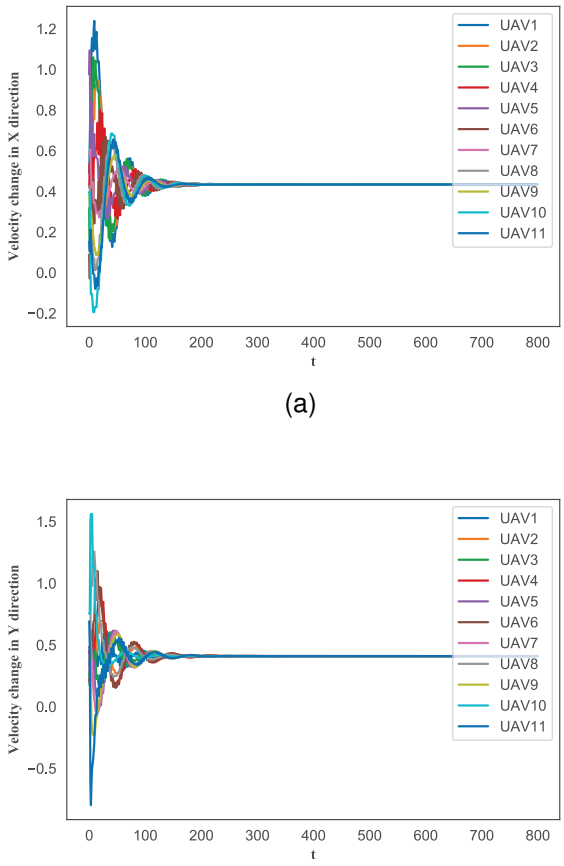

Fig. 9. The adjustment of velocities over switching topologies. (a) X dimension; (b) Y dimension.

C. Evaluation of the collision avoidance controller

This experiment evaluates the proposed collision avoidance controller. The experiment starts when multiple UAVs are in the status of formation flight, and an unknown and mobile obstacle intrudes the swarm. The key parameters are set as the same as before except the intruder. Through the experiments, we choose $\sigma = 1$, $\phi_a = 0.6$, $\phi_p = 0.3$,$\phi_n = 0.1$. These parameters show general examples. In practice, they should be set according to the deployment scenario and UAV hardware.

Fig. 10 shows six frames of the collision avoidance process. When the dynamic obstacle (denoted in red arrow) approaches the scope of the safe distance, the collision avoidance controller will direct the UAVs (denoted in blue dots; the blue line connecting the dots indicates the direction of movement) to avoid the obstacle flexibly, similar to starlings. In Fig. 10(a), the mobile obstacle begins to invade the formation. In Fig. 10(b), some UAVs that detect the obstacle begin to adopt the collision avoidance controller, and the remaining UAVs still operate the formation controller. Fig. 10(b)-(d) show the detailed process of evading the obstacle. Fig. 10(e)-(f) display that the formation is reformed after the collision avoidance stage.

The stability of the overall framework can be validated in Fig. 11, which illustrates the variation of the aggregation coefficient C during the formation and collision avoidance procedure. In the figure, the peak appears after the obstacle is detected. The bottom value shows that the swarm has the lowest density when multiple UAVs switch to the collision avoidance stage. The aggregation coefficient becomes stable again when the formation is reformed.

V. Conclusions

This paper proposes a distributed multiple-UAV control framework over fixed and switching topologies. We model each UAV using a second-order system and design two controllers to integrate formation flight and swarm intelligence into one framework, which takes inspiration from nature such as starlings. The UAVs can reach a desired formation based on the formation controller. When encountering mobile obstacles during voyage, they can flexibly evade it through the collision avoidance controller. To support the formation controller, this paper further gives the sufficient conditions of achieving an anticipated formation for both fixed and switching topologies. An aggregation coefficient is devised to demonstrate the stability of the system. Simulation experiments clearly show the performance of formation and collision avoidance for a general UAV swarm.

This paper provides a pioneering framework to integrate formation and swarm intelligence for UAV swarms. The proposed framework will be extended for more adverse scenarios where UAVs may have inaccurate or even faulty position information due to measurement failure, and the link quality is significantly

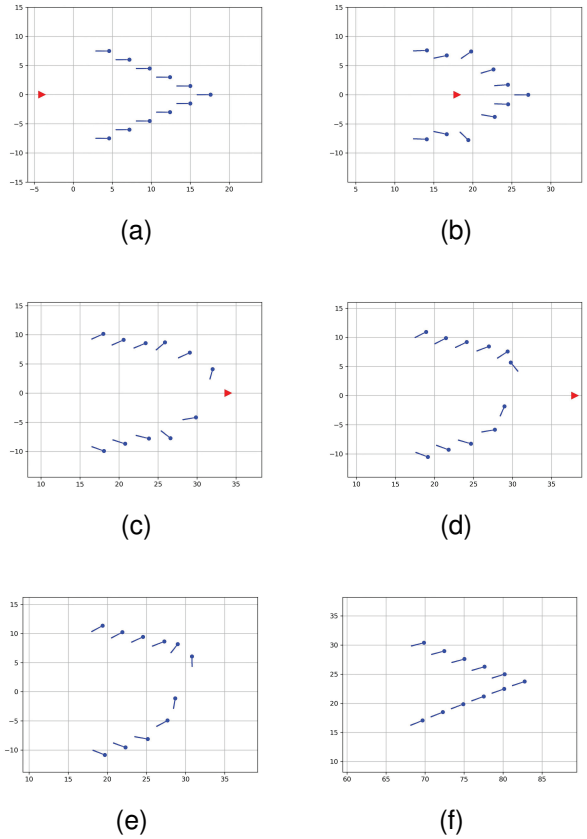

Fig. 10. Demonstration of the UAV swarm avoiding a mobile obstacle.

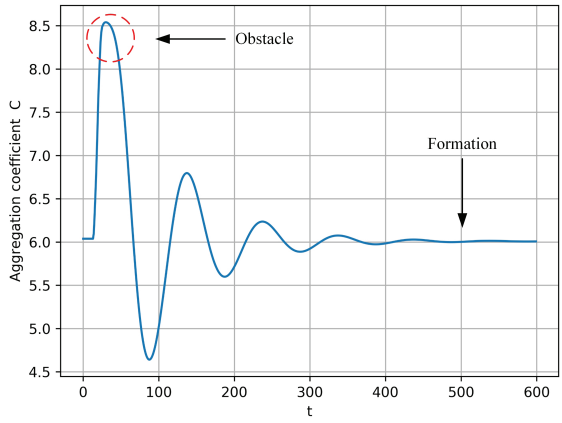

Fig. 11. Variation of the aggregation coefficient during the simulation experiment.

degraded due to interference and noise. Furthermore, the UAVs used in the framework are multi-rotors, which feature agile 3D movement in the space. For fixed-wing UAVs which are restricted by their physical dynamics, adaptation to the framework will be required, which is another promising research direction for future work.

The simulation experiment code of the proposed framework is accessible under request.

REFERENCES

[1] S. M. Adams and C. J. Friedland, "A survey of unmanned aerial vehicle (uav) usage for imagery collection in disaster research and management," in *9th International Workshop on Remote Sensing for Disaster Response*, vol. 8, 2011.

[2] G. Grenzdörffer, A. Engel, and B. Teichert, "The photogrammetric potential of low-cost uavs in forestry and agriculture," *The International Archives of the Photogrammetry, Remote Sensing and Spatial Information Sciences*, vol. 31, no. B3, pp. 1207–1214, 2008.

[3] P. Tokekar, J. Vander Hook, D. Mulla, and V. Isler, "Sensor planning for a symbiotic uav and ugv system for precision agriculture," *IEEE T. Robot.*, vol. 32, no. 6, pp. 1498–1511, 2016.

[4] M. Simic, C. Bil, and V. Vojisavljevic, "Investigation in wireless power transmission for uav charging," *Procedia Computer Science*, vol. 60, pp. 1846–1855, 2015.

[5] P. Waldron, "Why birds fly in a v formation," https://www.sciencemag.org/news/2014/01/why-birds-fly-v-formation, accessed January 15, 2014.

[6] G. Powell, "Experimental analysis of the social value of flocking by starlings (sturnus vulgaris) in relation to predation and foraging," *Anim. Behav.*, vol. 22, no. 2, pp. 501–505, 1974.

[7] X. Dong, B. Yu, Z. Shi, and Y. Zhong, "Time-varying formation control for unmanned aerial vehicles: Theories and applications," *IEEE T. Contr. Syst. T.*, vol. 23, no. 1, pp. 340–348, 2014.

[8] X. Ge and Q.-L. Han, "Distributed formation control of networked multi-agent systems using a dynamic event-triggered communication mechanism," *IEEE T. Ind. Electron.*, vol. 64, no. 10, pp. 8118–8127, 2017.

[9] H. Liu, T. Ma, F. L. Lewis, and Y. Wan, "Robust formation control for multiple quadrotors with nonlinearities and disturbances," *IEEE Trans. Cybern*, 2018.

[10] K. You and L. Xie, "Network topology and communication data rate for consensusability of discrete-time multi-agent systems," *IEEE T. Automat. Contr.*, vol. 56, no. 10, pp. 2262–2275, 2011.

[11] X. Liang, Y.-H. Liu, H. Wang, W. Chen, K. Xing, and T. Liu, "Leader-following formation tracking control of mobile robots without direct position measurements," *IEEE T. Automat. Contr.*, vol. 61, no. 12, pp. 4131–4137, 2016.

[12] X. You, C. Hua, and X. Guan, "Self-triggered leader-following consensus for high-order nonlinear multiagent systems via dynamic output feedback control," *IEEE Trans. Cybern*, vol. 49, no. 6, pp. 2002–2010, 2019.

[13] N. H. Li and H. H. Liu, "Formation uav flight control using virtual structure and motion synchronization," in *2008 American Control Conference*, pp. 1782–1787. IEEE, 2008.

[14] W. Ren and R. Beard, "Decentralized scheme for spacecraft formation flying via the virtual structure approach," *J Guid. Control. Dynam.*, vol. 27, no. 1, pp. 73–82, 2004.

[15] Z.-z. Yu, J.-h. Yan, J. Zhao, Z.-F. Chen, and Y.-h. Zhu, "Mobile robot path planning based on improved artificial potential field method," *Harbin Gongye Daxue Xuebao(Journal of Harbin Institute of Technology)*, vol. 43, no. 1, pp. 50–55, 2011.

[16] Y.-b. Chen, G.-c. Luo, Y.-s. Mei, J.-q. Yu, and X.-l. Su, "Uav path planning using artificial potential field method updated by optimal control theory," *Int. J. Syst. Sci.*, vol. 47, no. 6, pp. 1407–1420, 2016.

[17] C. Cutts and J. Speakman, "Energy savings in formation flight of pink-footed geese," *J Eep. Biol.*, vol. 189, no. 1, pp. 251–261, 1994.

[18] M. R. Bonyadi and Z. Michalewicz, "Analysis of stability, local convergence, and transformation sensitivity of a variant of the particle swarm optimization algorithm," *IEEE Trans. Evol. Comput.*, vol. 20, no. 3, pp. 370–385, 2015.

[19] M. R. Bonyadi, "A theoretical guideline for designing an effective adaptive particle swarm," *IEEE Trans. Evol. Comput.*, 2019.

[20] C. Fahy, S. Yang, and M. Gongora, "Ant colony stream clustering: A fast density clustering algorithm for dynamic data streams," *IEEE Trans. Cybern*, vol. 49, no. 6, pp. 2215–2228, 2018.

[21] C. W. Reynolds, *Flocks, herds and schools: A distributed behavioral model*, vol. 21, no. 4. ACM, 1987.

[22] G. Vásárhelyi, C. Virágh, G. Somorjai, T. Nepusz, A. E. Eiben, and T. Vicsek, "Optimized flocking of autonomous drones in confined environments," *Science Robotics*, vol. 3, no. 20, p. eaat3536, 2018.

[23] J. Cheng, W. Cheng, and R. Nagpal, "Robust and self-repairing formation control for swarms of mobile agents," in *AAAI*, vol. 5, no. 2005, 2005.

[24] X. Wang, V. Yadav, and S. Balakrishnan, "Cooperative uav formation flying with obstacle/collision avoidance," *IEEE T. Contr. Syst. T.*, vol. 15, no. 4, pp. 672–679, 2007.
[25] D. J. Pearce, A. M. Miller, G. Rowlands, and M. S. Turner, "Role of projection in the control of bird flocks," *P. Natl. Acad. Sci.*, vol. 111, no. 29, pp. 10 422–10 426, 2014.
[26] G. Wen, C. P. Chen, H. Dou, H. Yang, and C. Liu, "Formation control with obstacle avoidance of second-order multi-agent systems under directed communication topology," *Science China Information Sciences*, vol. 62, no. 9, p. 192205, 2019.
[27] Q. Shi, T. Li, J. Li, C. P. Chen, Y. Xiao, and Q. Shan, "Adaptive leader-following formation control with collision avoidance for a class of second-order nonlinear multi-agent systems," *Neurocomputing*, vol. 350, pp. 282–290, 2019.
[28] N. Ahmed, S. S. Kanhere, and S. Jha, "On the importance of link characterization for aerial wireless sensor networks," *IEEE Communications Magazine*, vol. 54, no. 5, pp. 52–57, 2016.
[29] K. Guo, X. Li, and L. Xie, "Ultra-wideband and odometry-based cooperative relative localization with application to multi-uav formation control," *IEEE transactions on cybernetics*, vol. 50, no. 6, pp. 2590–2603, 2019.
[30] S. Kang, M. Park, and H. Ahn, "Distance-based cycle-free persistent formation: Global convergence and experimental test with a group of quadcopters," *IEEE Transactions on Industrial Electronics*, vol. 64, no. 1, pp. 380–389, 2017.
[31] X. Dong, Y. Zhou, Z. Ren, and Y. Zhong, "Time-varying formation tracking for second-order multi-agent systems subjected to switching topologies with application to quadrotor formation flying," *IEEE Transactions on Industrial Electronics*, vol. 64, no. 6, pp. 5014–5024, 2017.
[32] W. Jasim and D. Gu, "Robust team formation control for quadrotors," *IEEE Transactions on Control Systems Technology*, vol. 26, no. 4, pp. 1516–1523, 2018.
[33] K. You and L. Xie, "Network topology and communication data rate for consensusability of discrete-time multi-agent systems," *IEEE T. Automat. Contr.*, vol. 56, no. 10, pp. 2262–2275, 2011.
[34] X.-D. Zhang, "Two sharp upper bounds for the laplacian eigenvalues," *Linear Algebra. Appl.*, vol. 376, pp. 207–213, 2004.
[35] C. Luo, W. Miao, H. Ullah, S. McClean, G. Parr, and G. Min, *Unmanned Aerial Vehicles for Disaster Management*, pp. 83–107. Singapore: Springer Singapore, 2019. [Online]. Available: https://doi.org/10.1007/978-981-13-0992-2_7
[36] C. Luo, S. I. McClean, G. Parr, L. Teacy, and R. De Nardi, "Uav position estimation and collision avoidance using the extended kalman filter," *IEEE Trans. Veh. Technol.*, vol. 62, DOI 10.1109/TVT.2013.2243480, no. 6, pp. 2749–2762, Jul. 2013.
[37] J. Tang, F. Zhu, and M. A. Piera, "A causal encounter model of traffic collision avoidance system operations for safety assessment and advisory optimization in high-density airspace," *Transportation research part C: emerging technologies*, vol. 96, pp. 347–365, 2018.
[38] J. Tang, M. A. Piera, and T. Guasch, "Coloured petri net-based traffic collision avoidance system encounter model for the analysis of potential induced collisions," *Transportation research part C: emerging technologies*, vol. 67, pp. 357–377, 2016.
[39] C. Fu, Q.-G. Wang, J. Yu, and C. Lin, "Neural network-based finite-time command filtering control for switched nonlinear systems with backlash-like hysteresis," *IEEE Transactions on Neural Networks and Learning Systems*, 2020.
[40] J. Yu, L. Zhao, H. Yu, and C. Lin, "Barrier lyapunov functions-based command filtered output feedback control for full-state constrained nonlinear systems," *Automatica*, vol. 105, pp. 71–79, 2019.
[41] J. Yu, P. Shi, and L. Zhao, "Finite-time command filtered backstepping control for a class of nonlinear systems," *Automatica*, vol. 92, pp. 173–180, 2018.
[42] R. Olfati-Saber and R. M. Murray, "Graph rigidity and distributed formation stabilization of multi-vehicle systems," in *Proceedings of the 41st IEEE Conference on Decision and Control, 2002.*, vol. 3, pp. 2965–2971. IEEE, 2002.